Polym. Bull. (2011) 67:1463–1481
DOI 10.1007/s00289-011-0466-3

Preparation of Cu/OMMT/LLDPE nanocomposites and synergistic effect study of two different nano materials in polymer matrix

Bing Xue · Fangfei Li · Yanping Xing · Mengmeng Sun · Darui Liu · Yinshan Jiang

Received: 7 August 2010 / Revised: 26 November 2010 / Accepted: 8 March 2011 /
Published online: 15 March 2011

Abstract Cu/OMMT (organo-montmorillonite)/LLDPE (linear low-density polyethylene) nanocomposites were prepared via melt mixing combined with melt extruding process. X-ray diffraction (XRD), Fourier-transform infrared (FTIR) spectra, scanning electron microscope (SEM), and transmission electron microscopy (TEM) were employed to characterize the resultant nanocomposites. The results showed that the OMMT layers were exfoliated and the nano-Cu particles were distributed uniformly in the polymer matrix. And the introduction of nanofiller into LLDPE matrix had little effect on the crystallinity of the polymer. The salt spray tests showed that OMMT and nano-Cu could improve the anticorrosion properties of LLDPE matrix, respectively. And the coexistence of OMMT and nano-Cu in Cu/OMMT/LLDPE nanocomposites could produce a synergistic effect on enhancing the anticorrosion properties. Furthermore, the co-incorporation of OMMT and nano-Cu into the polymer matrix also increased the thermal-oxidative stability and mechanical properties of LLDPE matrix significantly, as compared with the Cu/LLDPE and OMMT/LLDPE nanocomposites due to the synergistic effect. The bactericidal properties evaluation showed that the bactericidal ability of Cu/OMMT/LLDPE increases with nano-Cu content effectively.

Keywords Nanocomposites · Organo-montmorillonite · Nano-Cu · LLDPE · Synergistic effect

B. Xue · F. Li · M. Sun · D. Liu · Y. Jiang (✉)
Key Laboratory of Automobile Materials of Ministry of Education and Department of Materials Science and Engineering, Jilin University, Changchun 130025, China
e-mail: yinshan_jiang@yahoo.com.cn

Y. Xing
College of Animal Science and Veterinary Medicine Jilin University, 5333 Xi'an Road, Changchun 130062, China

Introduction

Maritime transportation of goods is an important part of our global economy. Because of aggressive marine atmosphere, corrosion protection packaging of metal products has become an important conduit of maritime transportation. Polyolefin packaging is a widely used method due to its good flexibility, considerable chemical resistance, and high transparency [1]. However, the organic packaging is not impermeable, widespread defects will create much small pathways for the corrosive species to reach packaged products, especially the metal products, and localized corrosion will occur [2]. The corrosion of metal products would become even worse under the aggressive marine atmosphere.

The addition of clays into polymer matrix is concerned to result in a remarkable improvement of mechanical resistance [3–6], thermal stability [4, 6], electrical conductivity and barrier properties mainly due to a tortuosity driven decreased in molecular diffusion of gases and vapors [7]. At present, PMMA [8, 9], polystyrene [10], polysulfone [11], epoxy resin [12], and polypyrrole [13] have been blended with organoclay or raw Na^+–MMT clay to create a series of novel polymer/MMT nanocomposites, which usually display advanced anticorrosion properties due to the physical barrier effect of MMT layers. Therefore, the more filler in polymer may result in the better anticorrosion effect. However, the excessive filler is difficult to be distributed uniformly in the polymer matrix, leading to significant decline in anticorrosion and mechanical properties [4].

Recently, a novel anticorrosion material, called static intercept material, was reported by Franey and Sutton [14]. Copper metal oxide used as functional filler is introduced into polymer matrix, where the copper metal oxide can react with corrosive acid gases, such as H_2S and HCl. So when these gases permeate into the anticorrosion material, they will be consumed by reacting with copper metal oxide. Copper metal oxide shows excellent anti-acid gases properties, but such functional filler is very expensive and has limited performance life. Once the functional filler is used up, the material would lose its corrosion protection ability for packed products. Meanwhile, we cannot ignore the fact that the static intercept material did not display a perfect performance in salt spray test [14] and limited its application in maritime anticorrosion packaging, although such material could provide perfect corrosion protection from corrosive acid gases.

As known, copper metal oxide could also be obtained by the oxidation of Cu in humid air. Therefore, if Cu powder is indirectly composed with polymers instead of copper metal oxide, Cu powder in packaging material may firstly react with permeated humid air and protect the packed products from salt spray. Meanwhile, the oxidation products of Cu in polymers may have similar anti-acid gases properties as static intercept material. Thus, such Cu/polymer may display anticorrosion property for both salt spray and acid gases. However, researches on such Cu/polymer anticorrosion materials are extremely rare.

It should be noted that, similar to static intercept material, Cu/polymer anti-corrosion materials are also limited by performance life especially in aggressive marine atmosphere. According to the discussions above, if MMT layers could be introduced into the Cu/polymer material to replace part of Cu powder, the physical

barrier properties of MMT layers would protect Cu/polymer to some extent, leading to remarkable increase in performance life and anticorrosion property of such material. Furthermore, since there are two different functional fillers in the polymer matrix, a smaller dosage of MMT and Cu would be adopted, resulting in more complete dispersion of MMT and much lower cost of such anticorrosion materials. However, studies on the anticorrosion properties and packing applications of Cu/MMT/polymer nanocomposite are much rarer.

In this work, Cu particles and OMMT were used to prepare Cu/OMMT/LLDPE novel anticorrosion nanocomposites. In order to improve the reaction activity of Cu in anticorrosion material, nano-scaled Cu powders were employed during preparation. X-ray diffraction (XRD), Fourier-transform infrared (FTIR), SEM, TEM, TG, salt spray test, mechanical properties test, and bactericidal experiment were used to evaluate the properties of Cu/OMMT/LLDPE nanocomposites. And the synergistic effect between nano-Cu and OMMT on the anticorrosion properties of resultant nanocomposites was also examined by thermal-oxidative stability analysis and mechanical performance test.

Experimental section

Chemical

Sodium pyrophosphate, cetyltrimethylammonium bromide (CTAB), silver nitrate, ultrafine copper oxide (mean diameter of 60 nm), absolute ethanol, and sulfuric acid are analytical pure reagents (AR) and purchased from the Shanghai Chemical Regents Company. Linear low-density polyethylene (LLDPE) is provided from Jilin Petrochemical. Compatilizer (maleic anhydride grafted linear low-density polyethylene) and antioxidant [*n*-otadecyl-*β*-(4-hydroxy-3,5-di-*tert*-butyl-phenyl)-propionate] are obtained from Nanjing Deba Chemical Co. Ltd. All chemicals are used as received without further purification. The Ca-montmorillonite (Ca-MMT) comes from Panshi country (Jilin province, China). The cation-exchange capacity (CEC) of the montmorillonite is 77 mmol per 100 g dry clay. This specimen is quite pure and little impurity is detected.

Preparation of organo-montmorillonite

The organo-montmorillonite was prepared by general method [15, 16]. After dispersion of 20.0 g of the clay in 1.0 L of distilled water, 8.5 g CTAB (corresponding to ~150% of the CEC) was added; the mixture was mechanically stirred for 2 h at 80 °C and then it was washed with distilled water. The washing process was repeated several times until the washings were free from bromide ions as indicated by $AgNO_3$. The prepared OMMT was dried at 80 °C, grounded with a mortar and then sieved. The 61 μm fraction was stored in a desiccator.

Preparation of nano-Cu

In a typical procedure of preparing nano-Cu, 20 g ultrafine CuO powder was calcined at 600 °C for 3 min. The moment of CuO powder was taken from Muffle furnace, it was carefully spread into 200 mL absolute ethanol. CuO powder underwent the following reaction [17]:

$$CH_3CH_2OH + CuO \rightarrow CH_3CHO + Cu + H_2O. \quad (1)$$

The mixture was filtered and immersed in 3 mol/L H_2SO_4 solution for 2 h. And then the red product was filtered, rinsed with absolute ethanol, and dried under vacuum at 50 °C.

Preparation of Cu/OMMT/LLDPE nanocomposites

Cu/OMMT/LLDPE nanocomposite was prepared via a two-step melt compounding process. First, nano-Cu, OMMT, compatilizer, antioxidant, and LLDPE were mixed in a SLJ-40 internal mixer (Education Apparatus Co., Changchun, China) at 170 °C for 30 min at the speed of 50 rpm. The total quantity of nano-Cu, OMMT, LLDPE, compatilizer, and antioxidant added into the internal mixer was 40 g. Second, sample removed from the internal mixer was extruded using a single-screw extruder (Education Apparatus Co., Changchun, China) at 170 °C at a screw speed of 50 rpm. For comparison, pure LLDPE was treated at the same compounding process. The denomination and composition of prepared nanocomposites was listed in Table 1.

Measurement

X-ray diffraction (XRD) study of prepared nano-Cu and nanocomposites was performed on an X' Pert PRO diffractometer with Cu Kα radiation (1.5418 Å) at 50 kV and 250 mA.

Fourier-transform infrared (FTIR) of the samples was carried out on a Nexus 670 auto Fourier transform infrared spectrometer for which samples were palletized with KBr powder.

Table 1 Composition of prepared nanocomposites

Samples	Nano-Cu (wt%)	OMMT (wt%)	LLDPE (wt%)	Compatilizer (wt%)	Antioxidant (wt%)
LLDPE	0	0	100	0	0
Cu4/LLDPE	4	0	90	5	1
Cu15/LLDPE	15	0	79	5	1
OMMT4/LLDPE	0	4	90	5	1
Cu3/OMMT1/LLDPE	3	1	90	5	1
Cu10/OMMT1/LLDPE	10	1	83	5	1
Cu20/OMMT1/LLDPE	20	1	73	5	1

Microscopic observations of nano-Cu and Cu/OMMT/LLDPE nanocomposites were performed in a Quanta200 environmental scanning electron microscope (SEM) and a JEM-1011 transmission electron microscopy (TEM).

The salt spray test, which could simulate ocean environment, was performed at a YW/R-150 salt mist corrosion testing box (Tianjin, China) according to ASTM B-117 (natural salt spray test) with the following conditions: the NaCl concentration of the sprayed solution was 50 g/L (5%NaCl) with the pH between 6.5 and 7.2, the temperature remained at 35 °C. Prepared nanocomposites and LLDPE were pressed into thin film with the thickness about 0.1 mm at an X-20 heat former machine (Education Apparatus Co., Changchun, China). The film was made into small bags with the size of 40 × 40 mm^2. Then, clean round iron (Q195 steel) coupons were sealed in the prepared bags. These bags were hung inside the testing box using plastic strings in a free standing mode to ensure that both sides of the bags got sprayed uniformly. After 168 h test duration, the samples were taken out from the chamber and the corrosion surface of the iron coupons was analyzed to evaluate the corrosion degree. In order to quantify the corrosion degree, corrosion rate of coupons was used as a reference. Here, corrosion rate was defined as a ratio between the area of rust on the coupons and the entire area of the coupons. The corrosion rate of coupons was obtained by calculating the pixel proportion of the rust in each photograph using Photoshop software. Considering the accuracy of software, the relative probable error was 10%.

In order to study the observable anticorrosion performance of nano-Cu particles in LLDPE matrix, Cu15/LLDPE with high content of nano-Cu was also tested by salt spray test. Because less corrosion product of nano-Cu was produced after salt spray test, only a large quantity of nano-Cu could produce enough corrosion products to be detected and distinguished between the changes in content. The distribution of corrosion product of nano-Cu in Cu15/LLDPE film after slat spray test was analyzed using XRD internal standard method. This method was based on the proportional relation between relative intensity and phase concentration [18]. Here, I/I_0 was defined as the relative intensity of corrosion product of nano-Cu, where I and I_0 represented the intensity of the strongest peak of corrosion product of nano-Cu and LLDPE phase, respectively. The outer surface of Cu15/LLDPE film was abraded on emery paper of 1200 meshes. The depth of abrasion was obtained by calculating the difference of thickness between the original Cu15/LLDPE film and the Cu15/LLDPE film after abrasion for each trial. The phases on the new exposed surface of Cu15/LLDPE film after abrasion were analyzed under identical diffraction conditions. So the relative intensity of corrosion product of nano-Cu was obtained from the XRD patterns of Cu15/LLDPE film at different depth of abrasion.

TG was carried on a WCT-2C thermoanalyzer (Optics Apparatus Co., Beijing, China). The samples were heated from ambient lab temperature (about 25 °C) to 800 °C at a rate of 15 °C/min under natural air atmosphere and Al_2O_3 as the inert reference.

The mechanical properties of the nanocomposites were evaluated by the tensile test and tear test at room temperature. Samples were cut to dumbbell shape according to ISO/R 527-1966E. The thickness of each sample was measured at six

different points with a micrometer and the average was taken. Samples were then drawn with a Universal Testing Machine (AG-IS, Shimadzu) at a stretching speed of 20 mm/min. The results presented were the mean values of six independent measurements.

The bactericidal properties of Cu/OMMT/LLDPE nanocomposites were evaluated using bacteria ATCC 25923 *Staphylococcus aureus* (*S. aureus.*) based on JIS Z2801:2000 standard. The Cu/OMMT/LLDPE nanocomposites were pressed into thin films and placed on a tray and then incubated with a calibrated bacterial suspension of *S. aureus.* The samples were then incubated at 37 °C for 8 h. After incubation, the antibacterial rate was calculated according to Eq. 2 to evaluate the bactericidal effect:

$$\text{Antibacterial rate} = (N_0 - N)/N_0 \times 100\% \quad (2)$$

where N_0 and N are the number of viable bacteria on a reference sample and Cu/OMMT/LLDPE thin films after antibacterial tests, respectively.

Results and discussion

Characterization of prepared nano-Cu and nanocomposites

Figure 1 shows the XRD pattern of prepared nano-Cu. As can be seen in Fig. 1, no new phase is found except Cu, indicating a pure product. The SEM photograph of nano-Cu is shown in Fig. 2. As shown in Fig. 2, the Cu particles have a spherical shape with a diameter lying in the range from 50 to 100 nm. The aggregation of nano-Cu might be formed because of their high surface energy caused by the size effect of nano-Cu.

It can be noted from the XRD pattern of OMMT (Fig. 3b) that the *d*-spacing of 2.153 nm is significantly larger than that of the untreated Ca-MMT, which has a *d*-spacing of 1.527 nm as indicated in Fig. 3a. The larger gallery spacing indicates the intercalation of alkyl ammonium between the silicate layers. The intercalation is also observed by FTIR measurements (Fig. 4). It can be seen that the C–H stretching vibration of alkyl ammonium chain appears at 2923 cm^{-1} and 2852 cm^{-1}, indicating the increase in hydrophobic property of resulting OMMT [19]. In Fig. 3c, no diffraction peak is shown, indicating that the OMMT layers are exfoliated. Figure 3d gives the typical XRD pattern of Cu/OMMT/LLDPE nanocomposite. The OMMT layers are also exfoliated as indicated by the disappearance of the OMMT diffraction peak.

Figure 5 shows the TEM results taken on specimen of the Cu3/OMMT1/LLDPE nanocomposite. The nanocomposite displays a highly dispersed morphology consisting of exfoliated OMMT layers of different size and spherical shape nano-Cu particles (see black arrows in Fig. 5), as well as a small amount of non-exfoliated OMMT aggregates. For preparing OMMT/polyolefin nanocomposites, a combination of appropriate organic modification [20–22] and sufficiently high shear forces in the melt during polymer processing is usually required to generate extensive ratios exfoliation in nanocomposites, however, fully exfoliated systems

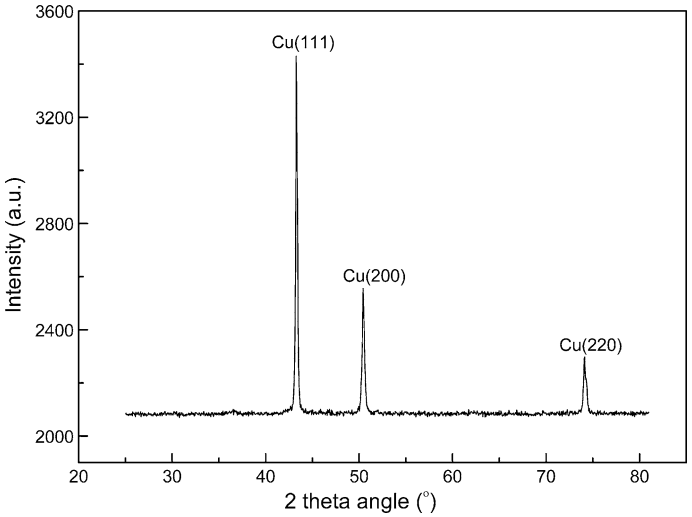

Fig. 1 XRD patterns of prepared nano-Cu

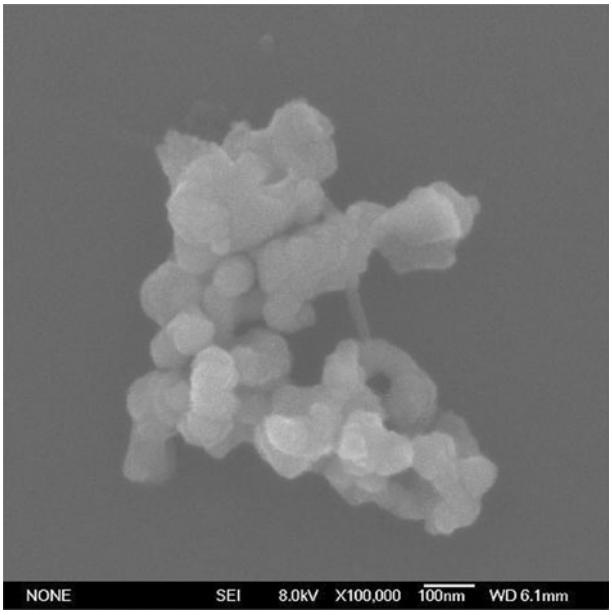

Fig. 2 SEM image of prepared nano-Cu

are very seldom achieved via conventional melt blending routes in polyolefin [23]. This nanocomposite appears to show, however, more highly dispersed exfoliated layers in the polyolefin matrix. Although there are clay aggregates in the microstructure of the nanocomposite, the thickness size of these in nanometer range has high aspect ratio to expect significant property improvements [24]. The

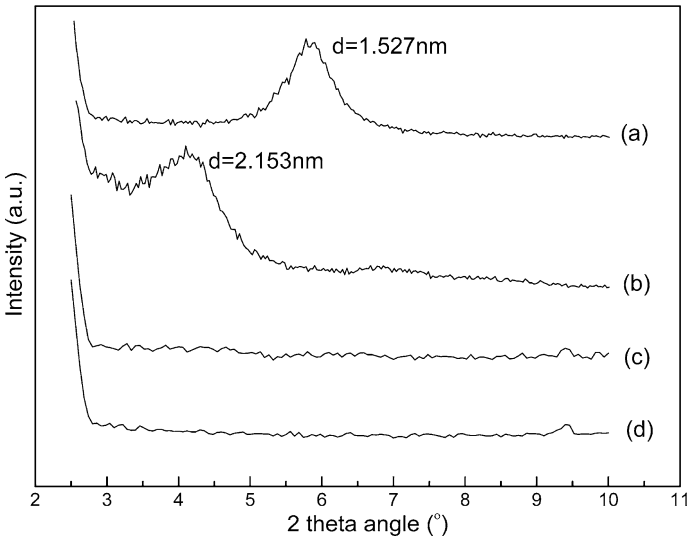

Fig. 3 XRD patterns in the range of 2θ angles from 2.5° to 10 ° for (*a*) original Ca-MMT, (*b*) OMMT, (*c*) OMMT4/LLDPE nanocomposite, (*d*) Cu3/OMMT1/LLDPE nanocomposite

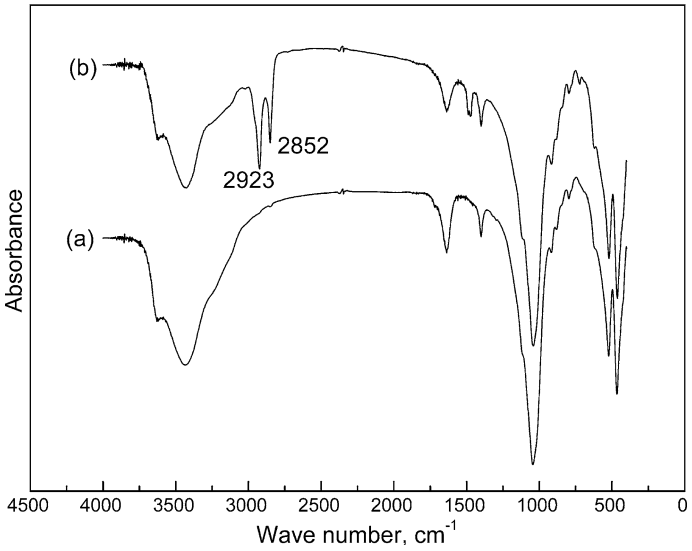

Fig. 4 FTIR spectra of (*a*) original Ca-MMT, (*b*) OMMT

actual aspect ratio (*L*/*T*) of the individual platelets is measured to be within 10 and 25, while for large aggregates, an average above 5 could be measured. It is observed in Fig. 5 that exfoliated layers appear to be an irregular orientation, however, there are still many exfoliated layers parallel to the nanocomposite surface. Non-exfoliated OMMT aggregates are prone to parallel to the nanocomposite surface.

This observation is quite similar to the case of dickite/LLDPE microcomposite we prepared previously [25]. Bigger layered particles in composite may be prone to be oriented at the process of hot press formation. In addition, it is been observed that the nano-Cu particles with mean diameter around 30 nm are distributed uniformly in the nanocomposite, indicating that high shear force during melt extrusion process may destroy the agglomeration of nano-Cu.

The effect of exfoliated clay and nano-Cu on the crystallinity of LLDPE is also analyzed by XRD diffraction patterns. In all samples, pronounced peaks from crystallographic planes (110) and (200) of LLDPE orthorhombic form are clearly visible, in Fig. 6 where the exemplary X-ray diffractograms are plotted for the respective range of 2θ angles. There are no noticeable differences between the samples studied. The crystallinity degree (determined as the ration of the area of the crystalline reflection to the total area of amorphous and crystalline reflections) and apparent crystalline sizes are listed in Table 2. As shown in Table 2, there are no observable variations in crystallinity degree and apparent crystalline sizes between LLDPE and prepared nanocomposites. Similar with LDPE [26], this behavior indicates no significant effect of exfoliated clay and nano-Cu on the crystallinity of LLDPE. Therefore, the number and types of fillers may be the most important factors that affect the composites properties.

Salt spray test

Performance in salt spray test

Figure 7 shows the photographs of iron coupon without and with a certain treatment. As iron cannot withstand the aggressive salt spray corrosion, the bare iron

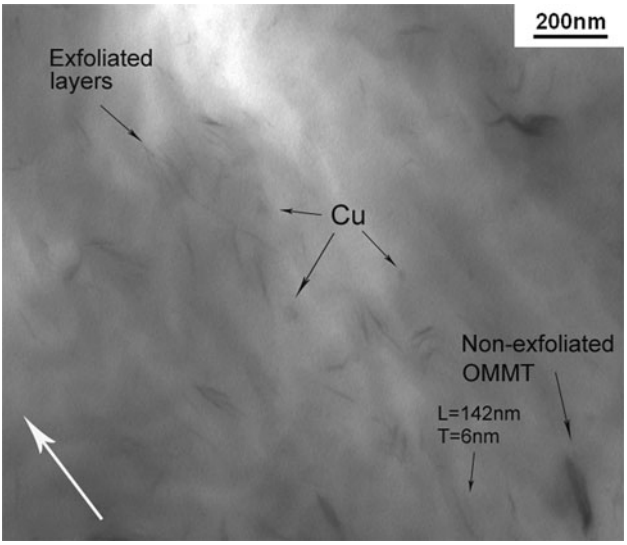

Fig. 5 TEM micrograph of Cu3/OMMT1/LLDPE nanocomposites

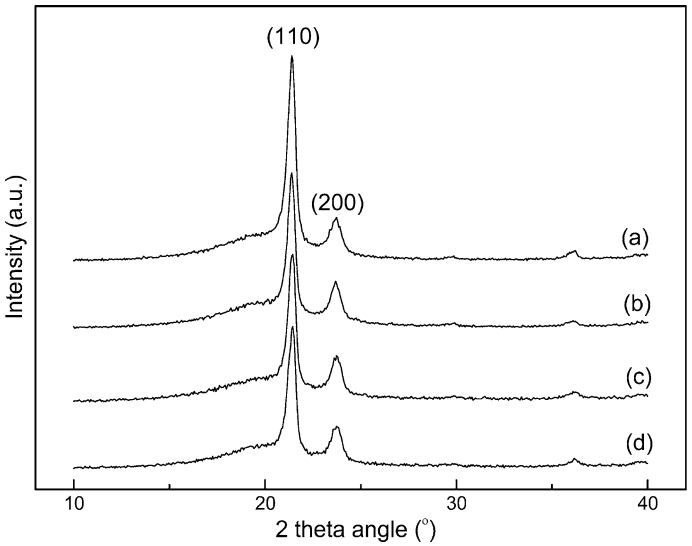

Fig. 6 XRD patterns in the range of 2θ angles from 10^{o} to 40^{o} for (*a*) LLDPE, (*b*) Cu4/LLDPE, (*c*) OMMT4/LLDPE, (*d*) Cu3/OMMT1/LLDPE nanocomposites

Table 2 Crystallinity degree and crystalline sizes of LLDPE, Cu4/LLDPE, OMMT4/LLDPE and Cu3/OMMT1/LLDPE nanocomposites

Sample	Crystallinity (%)	Crystalline sizes (Å)
LLDPE	56.43	170
Cu4/LLDPE	56.25	173
OMMT4/LLDPE	55.58	165
Cu3/OMMT1/LLDPE	55.39	172

coupon in testing box is badly corroded as shown in Fig. 7b and the corrosion rate is 100%. The corrosion rate of iron coupon packed with LLDPE bag has decreased to 23.0%. However, visible rust still appears on the surface of iron coupon. The introduction of OMMT or nano-Cu into LLDPE has improved the anticorrosion properties of this polymer. As shown in Fig. 7d, e, and f, the corrosion rate of these nanocomposites is no more than 2%. For the nanocomposites with same nano materials loadings, i.e. 4 wt%, the Cu3/OMMT1/LLDPE shows more excellent anticorrosion properties than either OMMT4/LLDPE or Cu4/LLDPE.

Anticorrosion mechanism of nano-Cu particles in LLDPE matrix

Figure 8 shows the XRD patterns of Cu15/LLDPE film before and after salt spray test. The peaks in Fig 8a corresponding to LLDPE and Cu, respectively, indicate a simple mixture of LLDPE and nano-Cu. After salt spray test, new peaks corresponding to Cu_2O appear in the XRD patterns of Cu15/LLDPE film (Fig. 8b, c). The appearance of Cu_2O is due to the fact that O_2 and H_2O can permeate into

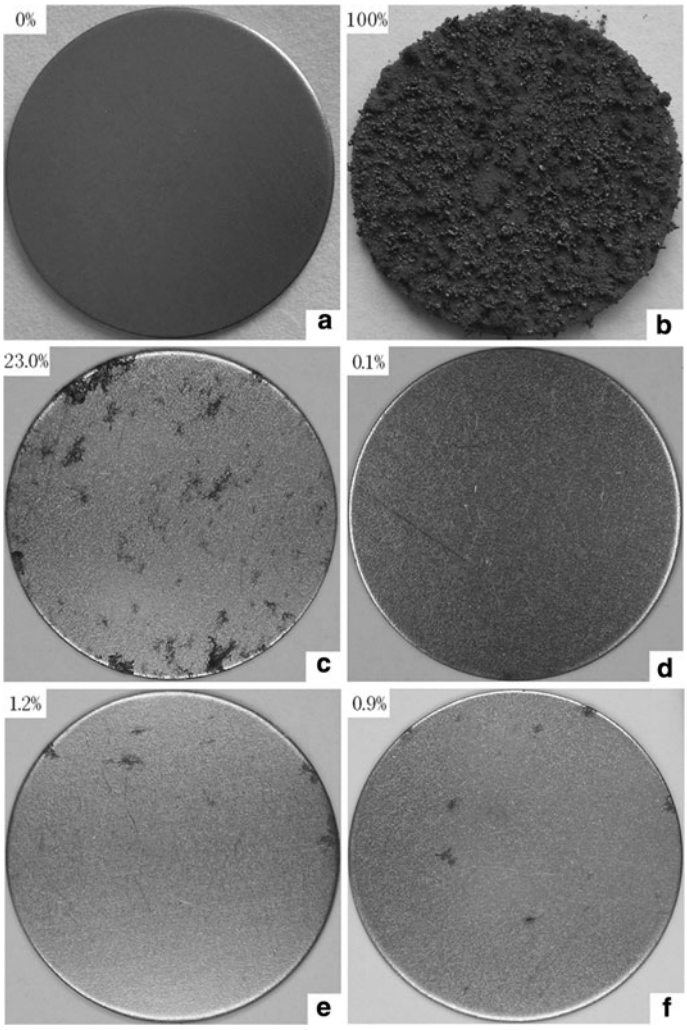

Fig. 7 Photographs of **a** original iron coupon, **b** bare iron coupon inside the testing box, iron coupon packed with **c** LLDPE bag, **d** Cu3/OMMT1/LLDPE bag, **e** OMMT4/LLDPE bag, **f** Cu4/LLDPE bag. Corrosion rate of iron coupon was marked on each photograph and the relative probable error was 10%

LLDPE matrix and corrode nano-Cu. Unlike bulk copper [27], the corrosion product of nano-Cu in Cu15/LLDPE film is Cu_2O. Cu nanoparticles may undergo the following reaction in testing box [28]:

$$2Cu + H_2O \rightarrow Cu_2O + 2H^+ + 2e^- \quad (3)$$

$$H_2O + (1/2)O_2 + 2e^- \rightarrow 2OH^- \quad (4)$$

$$4Cu + O_2 \rightarrow 2Cu_2O \quad (5)$$

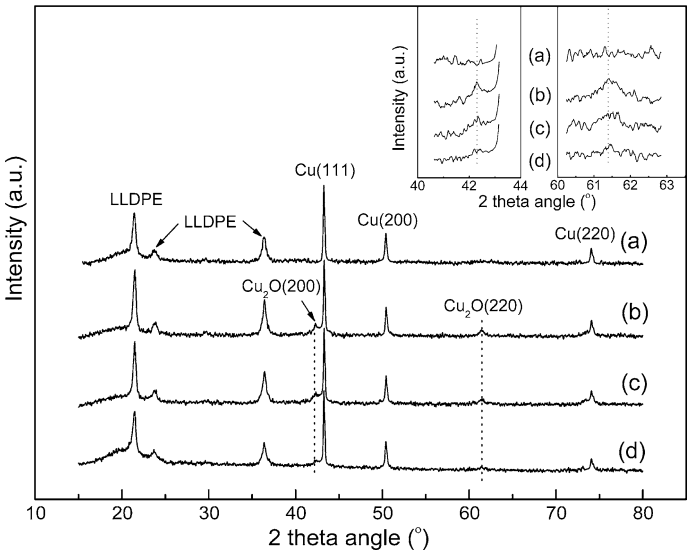

Fig. 8 XRD patterns of (*a*) Cu15/LLDPE film before salt spray test, (*b*) outer surface of Cu15/LLDPE film after salt spray test, (*c*) Cu15/LLDPE film at depth abrasion of 0.064 mm, (*d*) Cu15/LLDPE film at depth abrasion of 0.071 mm

As evident in Fig. 8b, c, and d, the characteristic diffraction peak intensity of Cu_2O varies with the depth of abrasion, indicating different content of Cu_2O in different depth of abrasion. Figure 9 displays a trend that the relative intensity of Cu_2O gradually reduced with the increasing of depth of abrasion. When the depth of abrasion reached about 0.07 mm, Cu_2O phase was hardly detected by XRD. As can be seen from Eqs. 3–5, the generation of Cu_2O in Cu15/LLDPE film can consume permeated O_2. So from the distribution of Cu_2O, it can be concluded that the permeation of O_2 gradually decreases. The nano-Cu particles in Cu/LLDPE nanocomposite have intercepted the permeation of O_2 and enhanced the anticorrosion properties of Cu/LLDPE nanocomposite.

Anticorrosion mechanism of Cu/OMMT/LLDPE nanocomposites

As seen from the TEM micrograph of Cu3/OMMT1/LLDPE nanocomposite in Fig. 5, exfoliated OMMT layers and spherical shape nano-Cu particles were highly dispersed in the nanocomposite. The high aspect ratio and nearly parallel orientation to the nanocomposite surface of exfoliated OMMT layers is beneficial to form a tortuous pathway, which retards the permeation of O_2 and H_2O through the nanocomposite film. The existence of exfoliated OMMT layers in LLDPE matrix could effectively improve the barrier properties of the nanocomposites [29, 30] and reduce the coefficient of diffusion of the gas and water molecules [31] by restricting the motion of polymer chains. Meanwhile, a small amount of permeated oxygen could be consumed by reacting with nano-Cu. In particular, permeation of water and oxygen along the formed tortuous pathway may result in more contacts between the

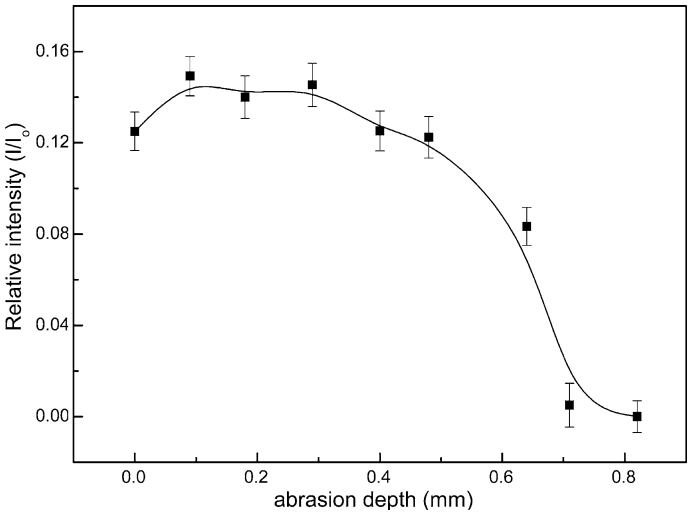

Fig. 9 Variation of relative intensity of Cu_2O phase with abrasion depth of Cu15/LLDPE film after salt spray test

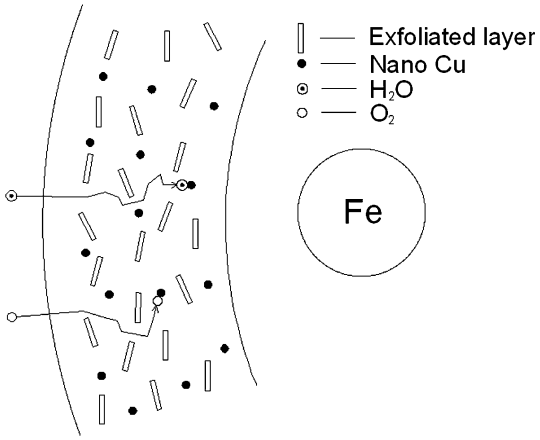

Fig. 10 Sketch of anticorrosion mechanism of Cu/OMMT/LLDPE nanocomposites

corrosive species and nano-Cu and ensure the more complete reaction according to Eqs. 3–5 (shown in Fig. 10). Thus, we draw the conclusion that the combination of physical barrier effect of OMMT and chemical consumption function of nano-Cu had played an important role in the improvement of the anticorrosion properties of Cu/OMMT/LLDPE nanocomposites.

Thermal-oxidative stability of Cu/OMMT/LLDPE nanocomposites

The TG curves of LLDPE, Cu4/LLDPE, OMMT4/LLDPE, and Cu3/OMMT1/LLDPE nanocomposites are shown in Fig. 11. Evidently, the onset of the thermal-oxidative decomposition of those composites shifts significantly toward the higher

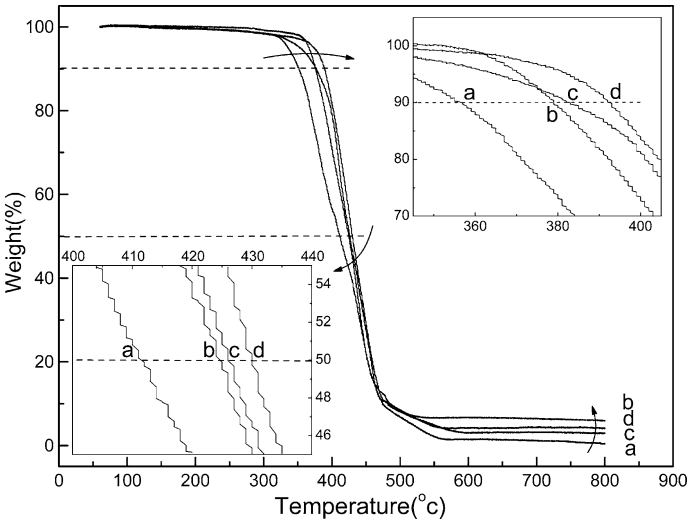

Fig. 11 TG curves of: (*a*) LLDPE, (*b*) Cu4/LLDPE, (*c*) OMMT4/LLDPE, (*d*) Cu3/OMMT1/LLDPE nanocomposites

temperature range than that of pure LLDPE, which shows the enhancement of thermal-oxidative stability of those nanocomposites [32]. The thermal-oxidative degradation temperatures corresponding to a mass loss of 10% ($T_{-10\%}$) and 50% ($T_{-50\%}$), respectively, are listed in Table 3. It can be seen that the prepared nanocomposites exhibit higher $T_{-10\%}$, $T_{-50\%}$ and lower mass loss (250–400 °C) value than that of pure LLDPE, indicating improved thermal-oxidative stability. Furthermore, it can also be seen that the Cu3/OMMT1/LLDPE demonstrates much higher thermal-oxidative stability than Cu4/LLDPE and OMMT4/LLDPE with the same clay content. When 4 wt% filler content is chosen, the $T_{-10\%}$ values of Cu4/LLDPE, OMMT4/LLDPE, and Cu3/OMMT1/LLDPE samples are 376, 379, and 391 °C, respectively.

For Cu3/OMMT1/LLDPE sample, the improvement in thermal-oxidative stability may depend on two facts. One is the formation of network [33] in the nanocomposites through polymer/nano-particle interactions generated from the larger surface area and surface energy of nano-Cu particles. The network formed through the fixation between the polymer chains and inorganic particles surface could result in an enhanced thermal-oxidative stability [34]. The other is due to the hindered effect of OMMT layers on the diffusion of oxygen and volatile products throughout the nanocomposites. This makes further contribution to the thermal-oxidative stability. Combination of these two effects could make the Cu/OMMT/LLDPE nanocomposites exhibit superior thermal-oxidative property with respect to the Cu/LLDPE and OMMT/LLDPE.

Mechanical properties of Cu/OMMT/LLDPE nanocomposites

The results of the mechanical properties of the prepared nanocomposites with various compositions are listed in Table 4. Compared with LLDPE, the introductions of nano

Table 3 TG data of LLDPE, Cu4/LLDPE, OMMT4/LLDPE and Cu3/OMMT1/LLDPE nanocomposites

Sample	$T_{-10\%}$ (°C)	$T_{-50\%}$ (°C)	Mass loss (250–400 °C) (%)
LLDPE	353	411	42
Cu4/LLDPE	376	424	29
OMMT4/LLDPE	379	426	19
Cu3/OMMT1/LLDPE	391	429	17

Table 4 Mechanical properties of LLDPE, Cu4/LLDPE, OMMT4/LLDPE and Cu3/OMMT1/LLDPE nanocomposites

Samples	Tensile strength[a] (MPa)	Tear strength[b] (kN/m)	Elongation at break[c] (%)
LLDPE	19.79	129.29	292
Cu4/LLDPE	21.68	130.43	279
OMMT4/LLDPE	22.95	129.31	303
Cu3/OMMT1/LLDPE	23.54	131.07	298

[a] Relative probable error 5%

[b] Relative probable error 2%

[c] Relative probable error 5%

materials into LLDPE matrix have improved the tensile and tear strength of the polymer generally. In particular, the reinforcement effect of Cu/OMMT is better than that of either Cu or OMMT as it can be seen from Table 4.

The reinforcement effect of the nano materials may be attributable to the following facts. The OMMT is found to be exfoliated in both OMMT4/LLDPE and Cu3/OMMT1/LLDPE as revealed by XRD measurements. For the OMMT/LLDPE nanocomposites, the improvement of the tensile and tear strength results from the delamination of the silicates in the LLDPE matrix and strong interactions between the polymer chains and the OMMT layers [35–37]. But, due to the layer shape of the exfoliated OMMT layers, the reinforcement could be anisotropic. The cracks along the direction of the OMMT layers may not be resisted. However, in the Cu/OMMT/LLDPE sample, the nano-Cu particles dispersed well in the LLDPE could bridge the cracks that are not stopped by the OMMT layers. As a result, coexistence of the exfoliated OMMT layers and the nano-Cu particles in the Cu/OMMT/LLDPE could produce a synergistic effect on reinforcing polymer matrix. The Cu/OMMT/LLDPE nanocomposites exhibit better enhanced mechanical properties than those of Cu/LLDPE and OMMT/LLDPE nanocomposites.

Antibacterial properties of Cu/OMMT/LLDPE nanocomposites

Figure 12 depicts the photos of bacterial colonies and antibacterial rate of Cu/OMMT/LLDPE with different filler content. It can be seen from Fig. 12b that the Cu3/OMMT1/LLDPE sample has a certain antibacterial effect and the bactericidal

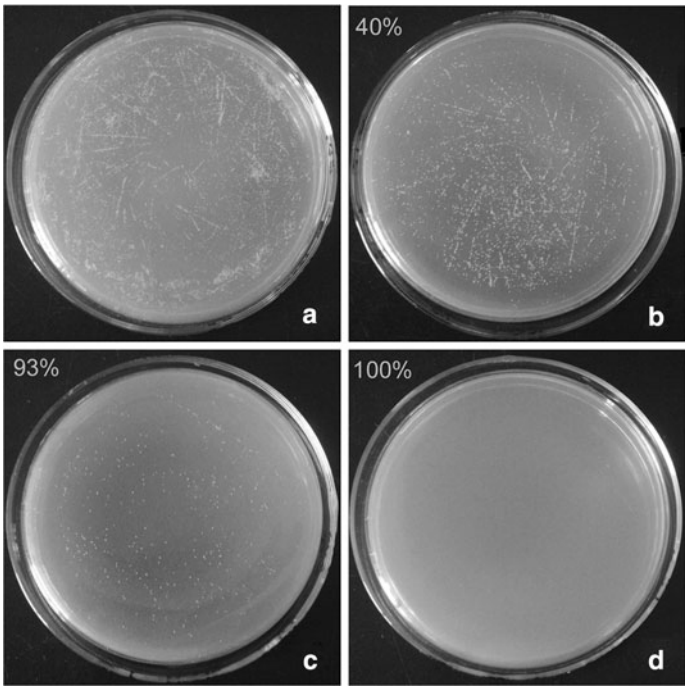

Fig. 12 Photos of the incubators after antibacterial testing: **a** reference sample, **b** Cu3/OMMT1/LLDPE, **c** Cu10/OMMT1/LLDPE, **d** Cu20/OMMT1/LLDPE

rate is about 40%. It is observed that the bactericidal ability increases with nano-Cu content effectively. In Fig. 12c, a bactericidal rate around 93% is achieved for 10 wt% nano-Cu loading. In this study, the Cu/OMMT/LLDPE with 20 wt% nano-Cu has an excellent antibacterial rate (Fig. 12d). The bactericidal effect of Cu/OMMT/LLDPE thin film is caused by the release of Cu ions when the nanocomposites contacting with water. Many assumptions have been proposed to explain the effects of elements such as copper, silver, etc. on the antibacterial properties. For instance, Knill et al. have proposed that the bacteria cell wall carries negative charges and positively charged copper may absorb on the cell wall and react with the cell wall. Thus, the cell wall will be damaged or the function of enzymes will be altered. The activity of the bacteria may be confined and finally the bacteria succumb [38, 39]. From this viewpoint, nanocomposites with high content of nano-Cu will release more Cu ions in aqueous solution, leading to an enhanced antibacterial effect. In addition, the well-dispersed OMMT layers in Cu/OMMT/LLDPE may hinder the release of Cu ions and improve the long-term antibacterial effect of the nanocomposites.

Conclusions

In the present work, we tried to use nano-Cu particles and OMMT to prepare novel anticorrosion material. The results of salt spray tests showed that nano-Cu in

LLDPE could improve the anticorrosion properties of the polymer matrix by reacting with permeated oxygen. In order to extend the performance life, reduce the cost and further improve the anticorrosion properties of the material, OMMT was introduced in LLDPE matrix. XRD measurements and TEM observations indicated that the OMMT layers were exfoliated and the nano-Cu particles were distributed uniformly in Cu/OMMT/LLDPE nanocomposites. The exfoliated OMMT layers enhanced the barrier properties of material and promoted the sufficient reaction between nano-Cu and corrosion species. Coexistence of the exfoliated OMMT layers and the nano-Cu particles in the Cu/OMMT/LLDPE nanocomposites could produce a synergistic effect on enhancing the thermal-oxidative stability and mechanical performance. Thermal analysis studies and mechanical tests results suggested that incorporating Cu/OMMT into the LLDPE matrix gave rise to much better enhanced thermal-oxidative stability and mechanical performance than incorporating either Cu or OMMT separately. Furthermore, it was observed that the bactericidal ability of Cu/OMMT/LLDPE nanocomposites increased with nano-Cu content effectively. Therefore, Cu/OMMT/LLDPE nanocomposites would be an effective and economical anticorrosion material for the application in maritime anticorrosion packaging.

Acknowledgments The authors are grateful for the financial support of the National Natural Science Foundation of China (grant No.50574043 and 40772028) and the supporting of Project 985-Automotive Engineering of Jilin University.

References

1. Lu HD, Hu Y, Li M, Chen ZY, Fan WC (2006) Structure characteristics and thermal properties of silane-grafted-polyethylene/clay nanocomposite prepared by reactive extrusion. Compos Sci Technol 66:3035–3039
2. Li P, Tan TC, Lee JY (1997) Corrosion protection of mild steel by electroactive polyaniline coatings. Synth Met 88:237–242
3. Chow WS, Mohd Ishak ZA (2007) Mechanical, morphological and rheological properties of polyamide 6/organo-montmorillonite nanocomposites. Express Polym Lett 1:77–83
4. Lee SY, Kang IA, Doh GH, Kim WJ, Kim JS, Yoon HG, Wu Q (2008) Thermal, mechanical and morphological properties of polypropylene/clay/wood flour nanocomposites. Express Polym Lett 2:78–87
5. Mojumdar SC, Raki L, Mathis N, Schimdt K, Lang S (2006) Thermal, spectral and AFM studies of calcium silicate hydrate-polymer nanocomposite material. Polym Bull 85:119–124
6. Chieng BW, Ibrahim NA, Wan Yunus WMZ (2010) Effect of organo-modified montmorillonite on poly(butylenes succinate)/poly(butylene adipate-co-terephthalate) nanocomposites. Express Polym Lett 4:404–414
7. Yu YH, Yeh JM, Liou SJ, Chang YP (2004) Organo-soluble polyimide (TBAPP–OPDA)/clay nanocomposite materials with advanced anticorrosive properties prepared from solution dispersion technique. Acta Mater 52:475–486
8. Yeh J-M, Liou S-J, Lin C-Y, Cheng C-Y, Chang Y-W, Lee K-R (2002) Anticorrosively enhanced PMMA–clay nanocomposite materials with quaternary alkylphosphonium salt as an intercalating agent. Chem Mater 14:154–161
9. Yeh J-M, Liou S-J, Lai M-C, Chang Y-W, Huang C-Y, Chen C-P, Jaw J-H, Tsai T-Y, Yu Y-H (2004) Comparative studies of the properties of poly(methyl methacrylate)-clay nanocomposite materials prepared by in situ emulsion polymerization and solution dispersion. J Appl Polym Sci 94:1936–1946

10. Yeh J-M, Liou S-J, Lin C-G, Chang Y-P, Yu Y-H, Cheng C-F (2004) Effective enhancement of anticorrosive properties of polystyrene by polystyrene-clay nanocomposite materials. J Appl Polym Sci 92:1970–1976
11. Yeh J-M, Chen C-L, Chen Y-C, Ma C-Y, Huang H-Y, Yu Y-H (2004) Enhanced corrosion prevention effect of polysulfone-clay nanocomposite materials prepared by solution dispersion. J Appl Polym Sci 92:631–637
12. Yeh J-M, Huang H-Y, Chen C-L, Su W-F, Yu Y-H (2006) Siloxane-modified epoxy resin–clay nanocomposite coatings with advanced anticorrosive properties prepared by a solution dispersion approach. Surf Coat Technol 200:2753–2763
13. Yeh J-M, Chin C-P, Chang S (2003) Enhanced corrosion protection coatings prepared from soluble electronically conductive polypyrrole-clay nanocomposite materials. J Appl Polym Sci 88:3264–3272
14. Franey PH, Sutton DM (2006) Static intercept* technology: a new packaging platform for corrosion and ESD protection. Bell Labs Tech J 11:137–146
15. Yuan XH, Li XH, Zhu E, Hu J, Cao SS, Sheng WC (2010) Synthesis and properties of silicone/montmorillonite nanocomposites by in situ intercalative polymerization. Carbohydr Polym 79:373–379
16. Sivudu KS, Thomas S, Shailaja D (2007) Synthesis and characterization of poly (4vp-co-dvb)/montmorillonite nanocomposites by in situ intercalative polymerization. Appl Clay Sci 37:185–192
17. Zheng HM, Liu XH, Yang SB, Wang X (2005) New approach for preparation of ultrafine Cu particles and shell/core compounds of Cu/CuO and Cu/Cu_2O. J Mater Sci 40:1039–1041
18. Ouhadi VR, Yong RN (2003) Impact of clay microstructure and mass absorption coefficient on the quantitative mineral identification by XRD analysis. Appl Clay Sci 23:141–148
19. Xu J, Li RKY, Xu Y, Li L, Meng YZ (2005) Preparation of poly(propylene carbonate)/organo-vermiculite nanocomposites via direct melt intercalation. Eur Polym J 41:881–888
20. Argun ME, Dursun S (2008) A new approach to modification of natural adsorbent for heavy metal adsorption. Bioresource Technol 99:2516–2527
21. Kornilov VM, Lachinov AN (2003) STM surface modification of the Si–SiO_2-polymer system. Microelectron Eng 69:399–404
22. Lemić J, Tomašević-Čanović M, Djuričić M, Stanić T (2005) Surface modification of sepiolite with quaternary amines. J Colloid Interface Sci 292:11–19
23. Sanchez-Garcia MD, Gimenez E, Lagaron JM (2008) Morphology and barrier properties of nano-biocomposites of poly(3-hydroxybutyrate) and layered silicates. J Appl Polym Sci 108:2787–2801
24. Park JH, Jana SC (2003) The relationship between nano- and micro-structures and mechanical properties in PMMA–epoxy–nanoclay composites. Polymer 44:2091–2210
25. Xue B, Jiang YS, Li FF, Xia MS, Sun MM, Liu DR, Zhang XG, Yu LX (2010) Hydrophobic modification of Dickite and salt spray test study on LLDPE/modified Dickite composite. J Appl Polym Sci 116:3408–3488
26. Morawiec J, Pawlak A, Slouf M, Galeski A, Piorkowska E, Krasnikowa N (2005) Preparation and properties of compatibilized LDPE/organo-modified montmorillonite nanocomposites. Eur Polym J 41:1115–1122
27. Chmielová M, Seidlerová J, Weiss Z (2003) X-ray diffraction phase analysis of crystalline copper corrosion products after treatment in different chloride solutions. Corros Sci 45:883–889
28. Tang LN, Wang FP (2008) Electrochemical evaluation of allyl thiourea layers on copper surface. Corros Sci 50:1156–1160
29. Chow WS (2007) Water absorption of epoxy glass fiber organo-montmorillonite nanocomposites. Express Polym Lett 1:104–108
30. Abacha N, Kubouchi M, Tsuda K, Sakai T (2007) Performance of epoxy-nanocomposite under corrosive environment. Express Polym Lett 1:364–369
31. Abacha N, Kubouchi M, Sakai T (2009) Diffusion behavior of water in polyamide 6 organoclay nanocomposites. Express Polym Lett 3:245–255
32. Yeh JM, Kuo TH, Huang HJ, Chang KC, Chang MY, Yang JC (2007) Preparation and characterization of poly(o-methoxyaniline)/Na^+–MMT clay nanocomposite via emulsion polymerization: electrochemical studies of corrosion protection. Eur Polym J 43:1624–1634
33. Yu TS, Lin JP, Xu JF, Ding WW (2005) Nanocomposites of vinyl chloride–acrylonitrile copolymer and silica. J Polym Sci Pol Phys 43:3127–3134
34. Dietsche F, Mulhaupt R (1999) Thermal properties and flammability of acrylic nanocomposites based upon organophilic layered silicates. Polym Bull 43:395–402

35. Choi YS, Choi MH, Wang KH (2001) Synthesis of exfoliated PMMA/Na-MMT nanocomposites via soap-free emulsion polymerization. Macromolecules 34:8978–8985
36. Krikorian V, Kurian M (2002) Polypeptide-based nanocomposite: structure and properties of poly (L-lysine)/Na^{+}-montmorillonite. J Polym Sci Pol Phys 40:2579–2586
37. Tyan H, Leu C, Wei K (2001) Effect of reactivity of organics-modified montmorillonite on the thermal and mechanical properties of montmorillonite/polyimide nanocomposites. Chem Mater 13:222–226
38. Knill CJ, Kennedy JF, Mistry J (2004) Alginate fibres modified with unhydrolysed and hydrolysed chitosans for wound dressings. Carbohydr Polym 55:65–76
39. Dan ZG, Ni HW, Xu BF, Xiong J, Xiong PY (2005) Microstructure and antibacterial properties of AISI 420 stainless steel implanted by copper ions. Thin Solid Films 492:93–100